

GWT + Bethe–Salpeter equation approach for photoabsorption spectra: Importance of self-consistent GWT calculations in small atomic systems

Riichi Kuwahara,^{1,2} Yoshifumi Noguchi,³ and Kaoru Ohno^{1,*}

¹ *Department of Physics, Yokohama National University,
79-5 Tokiwadai, Hodogaya-ku, Yokohama 240-8501, Japan*

² *Dassault Systèmes BIOVIA K.K., ThinkPark Tower,
2-1-1 Osaki, Shinagawa-ku, Tokyo 140-6020, Japan*

³ *Institute for Solid State Physics, The University of Tokyo,
5-1-5 Kashiwanoha, Kashiwa, Chiba 277-8581, Japan*

(Received 30 July 2015; Revised 29 June 2016)

Abstract

The self-consistent GWT method satisfies the Ward–Takahashi identity (i.e., the gauge invariance or the local charge continuity) for arbitrary energy (ω) and momentum (q) transfers. Its self-consistent first-principles treatment of the vertex $\Gamma = \Gamma_v$ or Γ_w is possible to first order in the bare (v) or dynamically-screened (w) Coulomb interaction. It is developed within a linearized scheme and combined with the Bethe–Salpeter equation (BSE) to accurately calculate photoabsorption spectra (PAS) and photoemission (or inverse photoemission) spectra (PES) simultaneously. The method greatly improves the PAS of Na, Na₃, B₂, and C₂H₂ calculated using the standard one-shot G_0W_0 + BSE method that results in significantly redshifted PAS by 0.8-3.1 eV, although the PES are well reproduced already in G_0W_0 .

The quasiparticle (QP) equation method in many-body perturbation theory [1] is powerful for simultaneously determining the photoemission (or inverse photoemission) spectra (PES), i.e., QP energy spectra, and QP wave functions of target materials from first-principles. In this method, we expand the skeleton diagrams, i.e., the diagrams drawn with the full Green's function lines, for the self-energy in terms of the electron-electron Coulomb interaction v , and solve the QP equation, which is equivalent to the Dyson equation, as a self-consistent (SC) eigenvalue problem. The Hartree–Fock (HF) approach provides the first-order approximation. In Hedin's set of equations [1] known as the GW Γ approach, the exchange-correlation part of the self-energy is expressed as $\Sigma_{\sigma}^{\text{xc}} = iG_{\sigma}W\Gamma_{\sigma}$, where G_{σ} and Γ_{σ} are the one-particle Green's function and the vertex function (σ is the spin index), respectively, and $W = (1 - vP)^{-1}v$ represents the dynamically screened Coulomb interaction ($P = -i\sum_{\sigma}G_{\sigma}G_{\sigma}\Gamma_{\sigma}$ is the polarization function). The simplest approximation is to assume $\Gamma_{\sigma} = 1$, which is called the GW approximation.

It is well known that the SC GW method usually overestimates the energy gap [2, 3], while the one-shot GW approach (G_0W_0) using the Kohn–Sham (KS) wave functions and eigenvalues [4] results in a better energy gap. However, quite recently, it has been pointed out that the photoabsorption spectra (PAS) for small molecules obtained by solving the Bethe–Salpeter equation (BSE) [5, 6] using G_0W_0 are often significantly redshifted by about 1 eV [7, 8]. The use of the Heyd–Scuseria–Ernzerhof (HSE) functional or the SC GW calculation (hereafter referred to as GW) improves the results, but they are not perfect [8, 9]. For a spin-polarized sodium atom (Na) and trimer (Na_3), G_0W_0 + BSE is extremely bad, although the G_0W_0 QP energies are reasonably good [10]. The calculated and experimental [11] optical gaps for Na are 1.32 eV and 2.10 eV, respectively, and the calculated and experimental [12] PAS for Na_3 are shown in Fig. 1. These calculated results are far off from the experimental data [13].

Here, we develop a GW Γ method, which involves a SC treatment of the vertex $\Gamma = \Gamma_v$ or Γ_w and satisfies the Ward–Takahashi identity [14–16] to first order in v or W , and show that it remarkably improves the QP energies and the optical gaps of spin-polarized Na, Na_3 , B_2 , and closed-shell C_2H_2 . In this method, the SC one-particle Green's function, i.e., SC QP energies and wave functions are obtained in the GW Γ scheme. We use the all-electron mixed basis approach, in which single particle wave functions are expanded with both plane waves (PWs) and atomic orbitals (AOs) [10, 17]. This Rapid Communication reports a first-principles SC GW Γ calculation and its application to the BSE, which has never been performed so far except for some recent reports of non-SC GW calculations including the second-order screened exchange by Ren *et al.*

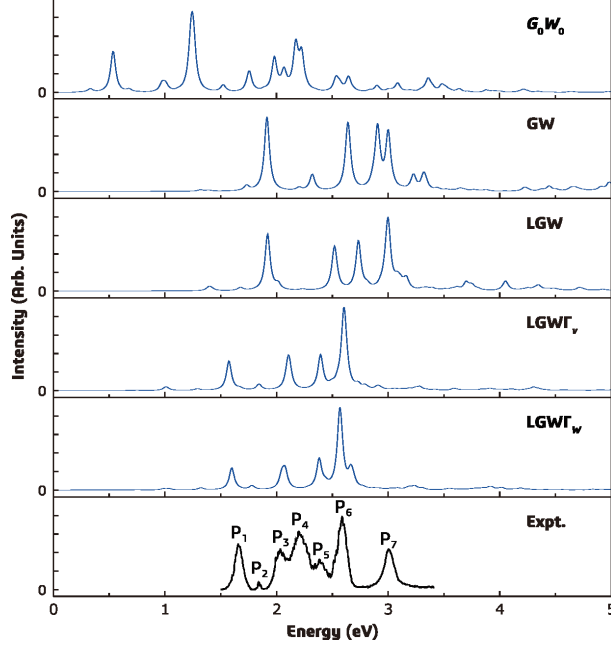


FIG. 1: Photoabsorption spectra of Na_3 calculated using G_0W_0 , GW, LGW, $\text{LGW}\Gamma_v$, and $\text{LGW}\Gamma_w$. Experimental data are taken from Ref. [12].

[18] and the GWT^1 method (i.e., $\text{GW}^{\text{TC-TC}}$ + single-shot vertex correction for the self-energy with the static approximation) by Grüneis *et al.* [19]. All these authors used the KS, HF, or HSE wave functions throughout the calculations.

In the present SC GWT + BSE calculations, we will show the following: (1) Highly reliable PES and PAS are simultaneously obtained for every system. (2) All calculated results deviate by 0.1 eV at most from the available experimental data. (3) The failure of the G_0W_0 + BSE calculations for the PAS is caused by the use of localized KS wave functions above the vacuum level (VL), and hence accurate QP wave functions are required.

Except for the G_0W_0 and GW calculations, we use our recently developed technique [17] to linearize the energy dependence of the self-energy $\Sigma_\sigma(\epsilon_n)$ to avoid the non-Hermitian problem caused by the energy dependence and to perform fully SC calculations. The important point of this technique is that $\Lambda_\sigma = \lim_{(\omega, q) \rightarrow 0} \Gamma_\sigma(\mathbf{r}_1, \mathbf{r}_2, \mathbf{q}; \mu + \omega, \mu) = 1 - \partial \Sigma_\sigma(\omega) / \partial \omega|_{\omega=\mu}$ is the vertex function in the limit $(\omega, q) \rightarrow 0$. This is the Ward–Takahashi identity in the same limit. [Here, $\mu = (\epsilon_{\text{HOMO}} + \epsilon_{\text{LUMO}})/2$.] The QP equation is given by $H_\sigma |n\sigma\rangle = \epsilon_{n\sigma} \Lambda_\sigma |n\sigma\rangle$ with $H_\sigma = \hat{T} + \hat{v}_{\text{nuc}} + \Sigma_\sigma(\mu) + \mu(\Lambda_\sigma - 1)$. Then, with the lower triangular matrix L_σ in the Choleski decomposition [20] $\Lambda_\sigma = L_\sigma L_\sigma^\dagger$, the renormalized QP states are given by $|\widetilde{n\sigma}\rangle = L_\sigma^\dagger |n\sigma\rangle$, which satisfy $\widetilde{H}_\sigma |\widetilde{n\sigma}\rangle = \epsilon_{n\sigma} |\widetilde{n\sigma}\rangle$

with $\tilde{H}_\sigma = L_\sigma^{-1} H_\sigma L_\sigma^{-1\dagger}$ as well as the orthogonality and completeness conditions. Moreover, the renormalized Green's function is given by $\tilde{G}_\sigma(\omega) = L_\sigma^\dagger G_\sigma(\omega) L_\sigma$; see Ref. [17] for more details.

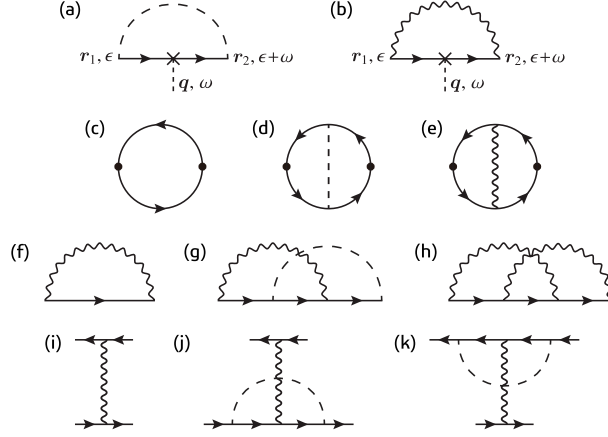


FIG. 2: Skeleton diagrams of the first-order vertex part (a) $\Gamma_{v\sigma}$ and (b) $\Gamma_{W\sigma}$; (c), (d), and (e) are the polarization part P ; (f), (g), and (h) are the exchange-correlation part of the self-energy $\Sigma_\sigma^{\text{xc}}$; (i), (j), and (k) are the interaction kernel $\tilde{T}^{\sigma_1\sigma'_1}$ of the BSE. (c), (f), and (i) are usual diagrams without vertex correction; (a), (d), (g), (j), and (k) involve the first-order vertex in v (dotted line); (b), (e), and (h) involve the first-order vertex in W (wavy line).

(*Theorem 1*) In this linearized formulation, we can additionally introduce the vertex part $\Gamma_{v\sigma}(\mathbf{r}_1, \mathbf{r}_2, \mathbf{q}; \epsilon + \omega, \epsilon)$ to first order in v [Fig. 2(a)], which we call the LGWT $_\nu$ method, or $\Gamma_{W\sigma}(\mathbf{r}_1, \mathbf{r}_2, \mathbf{q}; \epsilon + \omega, \epsilon)$ to first order in W [Fig. 2(b)], which we call the LGWT $_W$ method. These vertex parts depend fully on the energy and momentum transfers ω and \mathbf{q} , respectively, at the center (cross in those figures). See the Supplemental Material (SM) [21] for the proof of this theorem.

Then, the polarization function and the self-energy include the skeleton diagrams as shown in Figs. 2(c)-2(h). Figures 2(c) and 2(f) represent the diagrams without a vertex; Figs. 2(d) and 2(g) and Figs. 2(e) and 2(h) are the corresponding vertex corrections to first order in v ($\Gamma = \Gamma_v$) and W ($\Gamma = \Gamma_W$), respectively. Figure 3 illustrates the flow chart of the SC LGWT $_W$ method. The forms of the polarization function (Fig. 2(e)) and self-energy (Fig. 2(h)) are given in the SM.

(*Theorem 2*) The present LGWT $_\nu$ and LGWT $_W$ methods satisfy the generalized Ward–Takahashi identity for arbitrary ω and \mathbf{q} , which is equivalent to the gauge invariance (continuity equation for the electron density) [14–16], up to first order in v and W , respectively. The proof is

given in the SM.

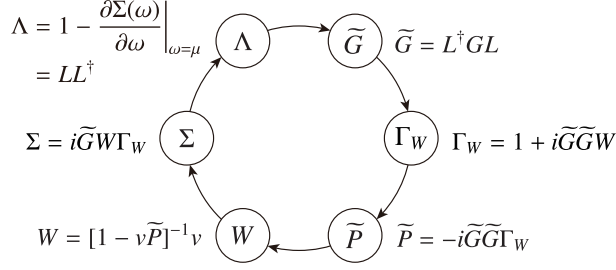


FIG. 3: Flow chart of the SC LGWT_W method. W and Γ_W are replaced by ν and Γ_ν in the SC LGWT _{ν} method.

Recently, the BSE has been solved in the one-shot second-order approach [22]. In what follows, we formulate the BSE for the LGWT _{ν} approach to spin-polarized systems. In the linearized formulation, we use the renormalized two-particle Green's function $\tilde{S}_{\sigma'_1\sigma'_2}^{\sigma_1\sigma_2}(x_1, x'_1; x_2, x'_2) = L_{\sigma'_1}L_{\sigma_1}^\dagger S_{\sigma'_1\sigma'_2}^{\sigma_1\sigma_2}(x_1, x'_1; x_2, x'_2)L_{\sigma_2}L_{\sigma'_2}^\dagger$ instead of $S_{\sigma'_1\sigma'_2}^{\sigma_1\sigma_2}(x_1, x'_1; x_2, x'_2)$, defined by subtracting $\delta_{\sigma_1\sigma'_1}\delta_{\sigma_2\sigma'_2}G(x_1, x'_1)G(x_2, x'_2)$ from the original two-particle Green's function. It satisfies the BSE

$$\begin{aligned}
\tilde{S}_{\sigma'_1\sigma'_2}^{\sigma_1\sigma_2}(x_1, x'_1; x_2, x'_2) &= \tilde{G}_{\sigma_1}(x_1, x_2)\tilde{G}_{\sigma'_1}(x'_2, x'_1)\delta_{\sigma'_1\sigma'_2}\delta_{\sigma_1\sigma_2} \\
&+ \sum_{\sigma_4\sigma'_4} \int \tilde{G}_{\sigma_1}(x_1, x_3) \frac{\delta \Sigma_{\sigma_3\sigma'_3}(x_3, x'_3)}{\delta \tilde{G}_{\sigma_4\sigma'_4}(x_4, x'_4)} \tilde{G}_{\sigma'_1}(x'_3, x'_1) (L_{\sigma'_4}L_{\sigma_4}^\dagger)^{-1} \\
&\times \tilde{S}_{\sigma'_4\sigma'_2}^{\sigma_4\sigma_2}(x_4, x'_4; x_2, x'_2) d^4x_3 d^4x'_3 d^4x_4 d^4x'_4,
\end{aligned} \tag{1}$$

where we used the fact that the original kernel $\Xi_{\sigma'_3\sigma'_4}^{\sigma_3\sigma_4}(x_3, x'_3; x_4, x'_4)$ is given by

$$\Xi_{\sigma'_3\sigma'_4}^{\sigma_3\sigma_4} = \frac{\delta \Sigma_{\sigma_3\sigma'_3}}{\delta G_{\sigma_4\sigma'_4}} = \frac{\delta \tilde{G}_{\sigma_3\sigma'_3}}{\delta G_{\sigma_3\sigma'_3}} \frac{\delta \Sigma_{\sigma_3\sigma'_3}}{\delta \tilde{G}_{\sigma_4\sigma'_4}} = L_{\sigma_3} \frac{\delta \Sigma_{\sigma_3\sigma'_3}}{\delta \tilde{G}_{\sigma_4\sigma'_4}} L_{\sigma'_3}^\dagger. \tag{2}$$

The functional derivative $\delta \Sigma_{\sigma_3\sigma'_3}(x_3, x'_3)/\delta \tilde{G}_{\sigma_4\sigma'_4}(x_4, x'_4)$ is given by $-i\delta_{\sigma_3\sigma'_3}\delta_{\sigma_4\sigma'_4}\delta(x_3 - x'_3)\delta(x_4 - x'_4)\nu(\mathbf{r}_3 - \mathbf{r}_4) + \delta_{\sigma_3\sigma_4}\delta_{\sigma'_3\sigma'_4}\tilde{I}^{\sigma_3\sigma'_3}(x_3, x'_3; x_4, x'_4)$. Ignoring all terms having functional derivatives of $W[\tilde{G}]$ with respect to \tilde{G} as usual [23], we have $\tilde{I}^{\sigma_3\sigma'_3}(x_3, x'_3; x_4, x'_4)$ expressed as $i\{\delta(x_3 - x_4)\delta(x'_3 - x'_4)W(x_3, x'_3) + \delta(x_3 - x_4)[W\Gamma_{\nu\sigma'_3}](x'_3, x'_4; x_3) + \delta(x'_3 - x'_4)[W\Gamma_{\nu\sigma_3}](x_3, x_4; x'_3)\}$, which is represented by the skeleton diagrams of Figs. 2(i), 2(j), and 2(k). Here the last two terms (Figs. 2(j) and 2(k)) come from vertex correction to first order in ν . From these equations, we find that $\Lambda_\sigma = L_\sigma L_\sigma^\dagger$ should be multiplied to the polarization function as $\tilde{P}_{\mathbf{G}\mathbf{G}'}^\sigma = P_{\mathbf{G}\mathbf{G}'}^\sigma \Lambda_\sigma$ [17]. Then, putting

$V_{\nu\mu dc}^{\sigma_1\sigma_2} = \sum_G \langle \nu\sigma_1 | e^{iG\cdot r} | \mu\sigma_1 \rangle \langle d\sigma_2 | e^{-iG\cdot r'} | c\sigma_2 \rangle v(G)$ and using the expression for $\widetilde{T}_{\nu\mu dc}^{\sigma_1\sigma'_1}(\omega)$ given in the SM, we obtain the matrix eigenvalue equation of the BSE [23]

$$(\epsilon_{c'\sigma_1} - \epsilon_{d'\sigma'_1} - \Omega_r) A_{d'\sigma'_1, c'\sigma_1}^r = - \sum_d^{\text{occ}} \sum_c^{\text{emp}} \left\{ \delta_{\sigma_1\sigma'_1} \sum_{\sigma_2} V_{c'd'dc}^{\sigma_1\sigma_2} A_{d\sigma_2, c\sigma_2}^r - \widetilde{T}_{c'd'dc}^{\sigma_1\sigma'_1}(\Omega_r) A_{d\sigma'_1, c\sigma_1}^r \right\} \quad (3)$$

in the Tamm–Dancoff approximation [23]. We also use this formulation in the LGWT_W approach, because the resulting error is on the order of 0.01 eV.

For spin-polarized systems, we have to generally solve the eigenvalue equation (3) in the $\uparrow\uparrow$ - $\downarrow\downarrow$ subspace,

$$\begin{pmatrix} h^{\uparrow\uparrow} + v^{\uparrow\uparrow} & v^{\uparrow\downarrow} \\ v^{\downarrow\uparrow} & h^{\downarrow\downarrow} + v^{\downarrow\downarrow} \end{pmatrix} \begin{pmatrix} A_{\uparrow\uparrow}^r \\ A_{\downarrow\downarrow}^r \end{pmatrix} = 0, \quad (4)$$

where we put $h^{\sigma_1\sigma'_1} = (\epsilon_{c'\sigma_1} - \epsilon_{d'\sigma'_1} - \Omega_r) \delta_{cc'} \delta_{dd'} - \widetilde{T}_{c'd'dc}^{\sigma_1\sigma'_1}$ and $v^{\sigma_1\sigma_2} = V_{c'd'dc}^{\sigma_1\sigma_2}$.

We used a face-centered cubic unit cell with edge length of 14 Å for Na and B₂, 15 Å for C₂H₂, and 18 Å for Na₃. All of the core and (truncated) valence numerical AOs are used together with the PWs. The atomic geometries are optimized with DMol³ [24, 25]. The bond lengths are 3.23 Å, 3.23 Å, and 5.01 Å for Na₃, 1.61 Å for B₂, 1.20 Å for C≡C, and 1.06 Å for C-H at the Becke three-parameter Lee-Yang-Parr (B3LYP) functional level. We used 3.61 (50.76) Ry, 1.23 (30.7) Ry, 6.82 (38.1) Ry, and 11.1 (44.2) Ry cutoff energies for PWs (for Σ_σ^x), respectively, for Na, Na₃, B₂, and C₂H₂. The cutoff energy for P and Σ_σ^c is the same as that for PWs for Na and Na₃, and is set at 4.57 Ry for B₂ and 3.98 Ry for C₂H₂. We used the full ω -integration [26] and the projection operator for the GW-related calculations, but used the plasmon-pole model [27] and 600 empty states for the Γ -related calculations as well as for solving the BSE in order to save the computational cost.

The resulting ionization potential (IP), electron affinity (EA), and optical gap E_g^{opt} (corresponding to the first dipole-allowed transition) of Na, Na₃, B₂, and C₂H₂ calculated using the G_0W_0 , GW, LGW, and LGWT_W methods are listed in Tables I and II, together with the results of previous multireference single and double configuration interaction (MRDCI) calculations [28–34], configuration interaction single and double (CID) calculations [35], and the corresponding experimental values [11, 12, 36–45]. For Na and Na₃, the results of LGWT_v are also listed in Table I. Note that EA of C₂H₂ is negative and not shown in Table II. Let us first compare the results of IP and EA with the experimental values. G_0W_0 results in reasonable IP and EA (IP of C₂H₂ is similar to those obtained in Ref. [46]) while GW has a tendency to overestimate IP and underestimate

EA, although the experimental error bar is large for B₂. LGW improves GW [17], but is not perfect. In contrast, LGWΓ_v and LGWΓ_w almost perfectly improve both IP and EA. For LGWΓ_w, the deviation from the experimental values is 0.03 eV for Na, 0.07 eV for Na₃, and 0.01 eV for C₂H₂. Compared with previous MRDCI calculations [28–32, 34], our results are closer to the experimental IP and EA for almost all cases.

TABLE I: Ionization potential (IP), electron affinity (EA), and optical gap E_g^{opt} (corresponding to $^2\text{S} \rightarrow ^2\text{P}$ and $^2\text{B}_2 \rightarrow ^2\text{A}_1$ transitions) of Na and Na₃ (in units of eV).

| | Na | | | Na ₃ | | |
|-------------------|-------------------|-------------------|--------------------|-------------------|------------------------|--------------------|
| | IP | EA | E_g^{opt} | IP | EA | E_g^{opt} |
| G_0W_0 | 5.15 | 0.41 | 1.32 | 4.10 | 1.14 | 0.53 |
| GW | 5.40 | 0.33 | 2.23 | 4.64 | 0.51 | 1.91 |
| LGW | 5.23 | 0.42 | 2.18 | 4.48 | 0.66 | 1.92 |
| LGWΓ _v | 5.01 | 0.60 | 2.00 | 4.08 | 1.04 | 1.57 |
| LGWΓ _w | 5.12 | 0.58 | 2.16 | 4.04 | 1.15 | 1.60 |
| MRDCI | 4.97 ^a | 0.44 ^b | 1.98 ^b | 3.76 ^c | 1.07/1.17 ^b | 1.61 ^b |
| Expt. | 5.14 ^d | 0.55 ^e | 2.10 ^f | 3.97 ^g | 1.02/1.16 ^h | 1.65 ⁱ |

^a Reference [28].

^b Reference [29].

^c Reference [30].

^d Reference [36].

^e Reference [37].

^f Reference [11].

^g Reference [38].

^h Reference [39].

ⁱ Reference [12].

Next we compare the results of the optical gap E_g^{opt} with experiments. G_0W_0 significantly underestimates the experimental E_g^{opt} for all systems and GW overestimates the experimental E_g^{opt} . The deviation from the experimental values is 0.8-3.1 eV for G_0W_0 and 0.13-0.26 eV for GW. LGW improves the results except for Na₃; the deviation from the experimental values is 0.08 eV for Na, 0.27 eV for Na₃, 0.04 eV for B₂, and 0.07 eV for C₂H₂. In contrast, LGWΓ_v and LGWΓ_w give excellent E_g^{opt} for all systems. For LGWΓ_w, the difference between the theoretical and experimental values is less than 0.06 eV for Na and Na₃, 0.05 eV for B₂, and 0.09 eV for C₂H₂. Compared with

TABLE II: IP, EA, and E_g^{opt} (corresponding to the $^3\Sigma_g^- \rightarrow ^3\Sigma_u^-$ transition) of B_2 , and IP and E_g^{opt} (corresponding to the $^1\Sigma_g^+ \rightarrow ^1\Pi_u$ transition) of C_2H_2 (in units of eV).

| | B_2 | | | C_2H_2 | |
|----------------------|-----------------------|----------------------|--------------------|------------------------|---------------------|
| | IP | EA | E_g^{opt} | IP | E_g^{opt} |
| G_0W_0 | 9.21 | 2.18 | 2.44 | 11.05 | 5.01 |
| GW | 9.97 | 1.76 | 3.94 | 11.65 | 8.39 |
| LGW | 9.79 | 1.94 | 3.75 | 11.44 | 8.23 |
| $\text{LGW}\Gamma_W$ | 9.87 | 1.91 | 3.84 | 11.48 | 8.25 |
| MRDCI | 9.48 ^a | 2.0 ^b | 3.85 ^c | 11.21 ^d | (8.06) ^e |
| Expt. | 10.3±0.6 ^f | 1.8±0.4 ^g | 3.79 ^h | 11.49 ⁱ | 8.16 ^j |

^a Reference [31].

^b Reference [32].

^c CASSCF/MRDCI: Reference [33].

^d Reference [34].

^e CID: Reference [35].

^f Reference [40].

^g Reference [41].

^h Reference [42, 43].

ⁱ Reference [44].

^j Reference [45].

the experimental values, our E_g^{opt} is better than the previous MRDCI results for Na [29], and CID results for C_2H_2 [35], or comparable to (differs only by 0.01 eV from) previous MRDCI results for Na_3 [29], and complete-active-space self-consistent-field (CASSCF)/MRDCI results for B_2 [33]. The $\text{LGW}\Gamma_W$ + BSE photoabsorption peak, i.e., the exciton wave function mainly consists of the following QP hole and electron level pair(s): $6(s\uparrow) \rightarrow 7(p\uparrow)$ for Na, $17(s\uparrow) \rightarrow 19(p\uparrow)$ for Na_3 , $4(\sigma\uparrow) \rightarrow 7(\pi\uparrow)$ and $3(\sigma\downarrow) \rightarrow 6(\pi\downarrow)$ for B_2 , and $7(\pi) \rightarrow 8(\sigma)$ for C_2H_2 . Figure 1 shows the PAS of Na_3 calculated using G_0W_0 , GW, LGW, $\text{LGW}\Gamma_v$, and $\text{LGW}\Gamma_W$ and the experimental spectra [12]. The overall spectral shapes are similar in all these methods except for G_0W_0 , although the peak positions are almost constantly shifted by an amount indicated by the difference between the calculated and experimental E_g^{opt} 's in Table I, and the peak heights somewhat change after the inclusion of the vertex correction. Obviously, GW and LGW overestimate the peak positions, while $\text{LGW}\Gamma_v$ and $\text{LGW}\Gamma_W$ give good peak positions except for P_4 and P_7 . ($\text{LGW}\Gamma_v$ has a small

peak at 2.9 eV, which may correspond to P_7 .) The remaining discrepancy between the theory and experiment in the case of Na_3 may be mainly attributed to the neglect of isomers and the atomic vibration effects.

Figure 4 shows the QP (or KS) energy spectra calculated using the local density approximation (LDA), G_0W_0 , and $\text{LGW}\Gamma_w$. The experimental IP and EA are indicated by IP and EA on the right vertical border line. Now we discuss the reason why the PAS calculated using G_0W_0 + BSE are so poor. For Na_3 , the number of up-spin (down-spin) levels below the VL is 26 (26) for LDA, 20 (19) for GW, 20 (20) for LGW, and 22 (20) for $\text{LGW}\Gamma_v$ and $\text{LGW}\Gamma_w$. We confirmed that the KS and QP wave functions very much resemble each other for the first 20 levels below the VL. However, they are quite different for the QP levels above the VL. For example, the spin-up and spin-down KS wave functions at the 21st down-spin level and the 23rd up-spin level below the VL are depicted in Fig. 4. They are localized. However, the corresponding G_0W_0 QP energies are both above the VL and the full QP wave functions are not localized. In our G_0W_0 + BSE calculation of Na_3 , the first small photoabsorption peak around 0.35 eV (see the top panel in Fig. 1) mainly consists of the QP hole and electron level pairs between $16 \rightarrow 17$ (19.8%), 21 (8.7%) for down-spin, and $17 \rightarrow 18$ (21.8%), 20 (31.4%), 21 (9.0%), 23 (2.3%) for up-spin. The unphysically bound KS wave functions of the $21\downarrow$ and $23\uparrow$ levels contribute to the BSE matrix elements, leading to unphysically large electron-hole interactions and in turn, to the optical transitions with very small photoabsorption energies. This gives the wrong spectra for G_0W_0 in Fig. 1. It has already been known for more than 50 years [47] that the BSE should be solved with the fully SC Green's function in order to satisfy the conservation laws as well as the longitudinal f -sum rule. However, the QP gap and the optical gap obtained using the GW method are blueshifted because they do not satisfy the generalized Ward–Takahashi identity. To improve the result, it is necessary to use the GWT method.

In this Rapid Communication, we presented the G_0W_0 , GW, LGW, and $\text{LGW}\Gamma_w$ ($\text{LGW}\Gamma_v$) calculations for Na, Na_3 , B_2 , and C_2H_2 . If the G_0W_0 QP energies are used together with the KS wave functions, there is inconsistency between the QP energies and wave functions at some levels above the VL. Moreover, the GW and LGW methods are not sufficient because they overestimate both the QP energy gap and optical gap. To obtain better gap estimates, it is necessary to perform the GWT calculation. We showed that the $\text{LGW}\Gamma_w$ method produces consistent and the best PES and PAS among all of the methods used in this study. The self-consistent treatment of Γ is required to obtain consistently good results for both PES and PAS, and its computational cost scales as

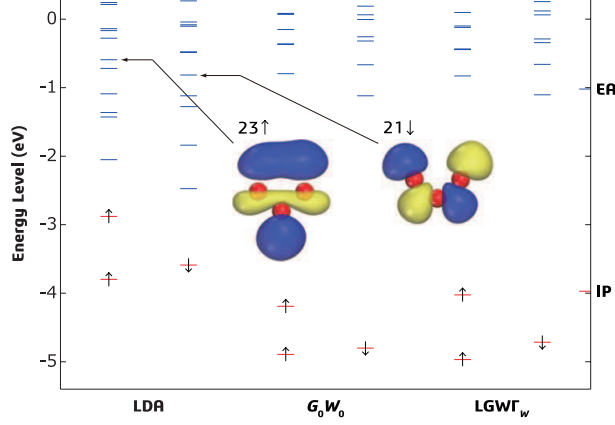


FIG. 4: QP (or KS) energy spectra of Na_3 calculated using the LDA, G_0W_0 , and $\text{LGW}\Gamma_w$. Unphysically bound KS wave functions at the 21st spin-down level and the 23rd spin-up level are also depicted. Red balls are Na atoms, while yellow and blue colors indicate the positive and negative regions of the wave function, respectively.

$O(N^2M^3)$, where N and M are the numbers of basis functions and empty states, respectively, if we use the plasmon-pole model. The present method is applicable to vertical transitions but cannot handle relaxation processes.

This work was supported by the Grant-in-Aid for Scientific Research B (Grant No. 25289218) from JSPS and also by the Grant-in-Aid for Scientific Research on Innovative Areas (Grant No. 25104713) from MEXT. We are also indebted to the HPCI promoted by MEXT for the use of the supercomputer SR16000 at Hokkaido University and at IMR, Tohoku University (Project IDs. hp140214, hp150231, hp160072, and hp160234).

* ohno@ynu.ac.jp

- [1] L. Hedin, Phys. Rev. **139**, A796 (1965).
- [2] T. Kotani, M. van Schilfgaarde, and S. V. Faleev, Phys. Rev. B **76**, 165106 (2007).
- [3] M. Shishkin, M. Marsman, and G. Kresse, Phys. Rev. Lett. **99**, 246403 (2007).
- [4] M. S. Hybertsen and S. G. Louie, Phys. Rev. Lett. **55**, 1418 (1985).
- [5] G. Onida, L. Reining, R. W. Godby, R. Del Sole, and W. Andreoni, Phys. Rev. Lett. **75**, 818 (1995).
- [6] M. Rohlfing and S. G. Louie, Phys. Rev. Lett. **80**, 3320 (1998).

- [7] D. Hirose, Y. Noguchi, and O. Sugino, Phys. Rev. B **91**, 205111 (2015).
- [8] D. Jacquemin, I. Duchemin, X. Blase, J. Chem. Theory Comput. **11**, 3290 (2015).
- [9] F. Bruneval, S. M. Hamed, and J. B. Neaton, J. Chem. Phys. **142**, 244101 (2015).
- [10] Y. Noguchi, S. Ishii, K. Ohno, and T. Sasaki, J. Chem. Phys. **129**, 104104 (2008).
- [11] J. E. Sansonetti, J. Phys. Chem. Ref. Data **37**, 1659 (2008).
- [12] C. R. C. Wang, S. Pollack, T. A. Dahlseid, G. M. Koretsky, and M. M. Kappes, J. Chem. Phys. **96**, 7931 (1992).
- [13] For the even number clusters of sodium, the G_0W_0 + BSE result is not so bad; see Ref. [5] and: Y. Noguchi and K. Ohno, Phys. Rev. A **81**, 045201 (2010).
- [14] J. C. Ward, Phys. Rev. **78**, 182 (1950);
- [15] Y. Takahashi, Il Nuovo Cimento **6**, 371 (1957).
- [16] J. R. Schrieffer, *Theory of Superconductivity* (Advanced Book Classic) (Westview Press, 1999) Chap. 8-5.
- [17] R. Kuwahara and K. Ohno, Phys. Rev. A. **90**, 032506 (2014).
- [18] X. Ren, P. Rinke, G. E. Scuseria, and M. Scheffler, Phys. Rev. B **88**, 035120 (2013).
- [19] A. Grüneis, G. Kresse, Y. Hinuma, and F. Oba, Phys. Rev. Lett. **112**, 096401 (2014).
- [20] It is also possible to use $L = \Lambda^{1/2}$ instead of the Choleski decomposition in the linearization procedure as in Ref. [3].
- [21] See Supplemental Material at <http://link.aps.org/supplemental/10.1103/PhysRevB.xx.xxxxxx> for the proof of Theorem 1 and Theorem 2.
- [22] D. Zhang, S. N. Steinmann, and W. Yang, J. Chem. Phys. **139**, 154109 (2013).
- [23] G. Strinati, Phys. Rev. Lett. **49**, 1519 (1982).
- [24] B. Delley, J. Chem. Phys. **92**, 508 (1990).
- [25] B. Delley, J. Chem. Phys. **113**, 7756 (2000).
- [26] M. Zhang, S. Ono, N. Nagatsuka, and K. Ohno, Phys. Rev. B **93**, 155116 (2016).
- [27] W. von der Linden and P. Horsch, Phys. Rev. B **37**, 8351 (1988).
- [28] R. J. Buenker and S. Krebs, in *Recent Advances in Multireference Methods*, edited by K. Hirao, Recent Advances in Computational Chemistry Vol. 4 (World Scientific, Singapore, 1999) pp.1-29.
- [29] V. Bonačić-Koutecký, P. Fantucci, and J. Koutecký, J. Chem. Phys. **93**, 3802 (1990).
- [30] V. Bonačić-Koutecký, I. Boustani, M. Guest, and J. Koutecký, J. Chem. Phys. **89**, 4861 (1988).
- [31] P. J. Bruna and J. S. Wright, J. Phys. Chem. **94**, 1774 (1990).

- [32] P. J. Bruna and J. S. Wright, J. Phys. B **23**, 2197S (1990).
- [33] S. R. Langhoff and C. W. Bauschlicher, Jr., J. Chem. Phys. **95**, 5882 (1991).
- [34] W. P. Kraemer and W. Koch, Chem. Phys. Lett. **212**, 631 (1993).
- [35] W. E. Kammer, Chem. Phys. **5**, 408 (1974).
- [36] A. Herrmann, E. Schumacher, and L. Wöste, J Chem. Phys. **68**, 2327 (1978).
- [37] H. Hotop and W. C. Lineberger, J. Phys. Chem. Ref. Data **14**, 731 (1985).
- [38] A. Herrmann, S. Leutwyler, E. Schumacher, and L. Woste, Helv. Chim. Acta **61**, 453 (1978).
- [39] K. M. McHugh, J. G. Eaton, G. H. Lee, H. W. Sarkas, L. H. Kidder, J. T. Snodgrass, M. R. Manaa, and K. H. Bowen, J. Chem Phys. **91**, 3792 (1989).
- [40] L. Hanley, J. L. Whitten, and S. L. Anderson, J. Phys. Chem. **92**, 5803 (1988).
- [41] C. J. Reid, Int. J. Mass Spect. Ion Proces. **127**, 147 (1993).
- [42] W. R. M. Graham and W. Weltner Jr., J. Chem. Phys. **65**, 1516 (1976).
- [43] K. P. Huber and G. Herzberg, *Molecular Spectra and Molecular Structure: IV. Constants of Diatomic Molecules* (Van Nostrand Reinhold Company, New York, 1979).
- [44] G. Bieri and L. Åsbrink, J. Elec. Spec. Rel. Phenom. **20**, 149 (1980).
- [45] W. C. Price, Phys. Rev. **47**, 444 (1935).
- [46] M. J. van Setten, F. Caruso, S. Sharifzadeh, X. Ren, M. Scheffler, F. Liu, J. Lischner, L. Lin, J. R. Deslippe, S. G. Louie, C. Yang, F. Weigend, J. B. Neaton, F. Evers, and P. Rinke, J. Chem. Theory Comput. **11**, 5665 (2015).
- [47] G. Baym and L. P. Kadanoff, Phys. Rev. **124**, 287 (1961).

Supplemental Material

* * * * *

GW Γ + Bethe–Salpeter equation approach for photoabsorption spectra: Importance of self-consistent GW Γ calculations in small atomic systems

* * * * *

Riichi Kuwahara,^{1,2} Yoshifumi Noguchi,³ and Kaoru Ohno^{1,*}

¹ *Department of Physics, Yokohama National University,
79-5 Tokiwadai, Hodogaya-ku, Yokohama 240-8501, Japan*

² *Dassault Systèmes BIOVIA K.K., ThinkPark Tower,
2-1-1 Osaki, Shinagawa-ku, Tokyo 140-6020, Japan*

³ *Institute for Solid State Physics, The University of Tokyo,
5-1-5 Kashiwanoha, Kashiwa, Chiba 277-8581, Japan*

In this Supplemental Material, we prove Theorem 1 and Theorem 2, and present explicit forms of the polarization function, the self-energy, and the interaction kernel $\tilde{T}_{\nu\mu dc}^{\sigma_1\sigma'_1}(\omega)$. Figure and reference numbers refer to the figures and references in the Letter except for Ref [S1].

Theorem 1. In the linearized formulation, one can additionally introduce the vertex part $\Gamma_{\nu\sigma}(\mathbf{r}_1, \mathbf{r}_2, \mathbf{q}; \epsilon + \omega, \epsilon)$ at the first order in the bare Coulomb interaction ν (Fig. 2(a)), which we will call the LGWT $_{\nu}$ method, or $\Gamma_{W\sigma}(\mathbf{r}_1, \mathbf{r}_2, \mathbf{q}; \epsilon + \omega, \epsilon)$ at the first order in the dynamically screened Coulomb interaction W (Fig. 2(b)), which we will call the LGWT $_W$ method.

Theorem 2. The LGWT $_{\nu}$ and LGWT $_W$ methods satisfy the Ward–Takahashi identity to the first order in the bare Coulomb interaction ν and in the dynamically screened Coulomb interaction W , respectively.

PROOF OF THEOREM 1

The statement of Theorem 1 holds because using $\widetilde{G}_\sigma(\omega)$ in place of $G_\sigma(\omega)$ in the linearized formulation introduces the $\omega = \mathbf{q} = 0$ vertex function Λ_σ just at the other side of the interaction line where we introduced the first-order vertex part $\Gamma_{v\sigma}(\mathbf{r}_1, \mathbf{r}_2, \mathbf{q}; \epsilon + \omega, \epsilon)$ or $\Gamma_{W\sigma}(\mathbf{r}_1, \mathbf{r}_2, \mathbf{q}; \epsilon + \omega, \epsilon)$ for arbitrary ω and \mathbf{q} . Therefore there is no double counting in the vertex correction up to the first order in v or W . In this way, the LGWT $_v$ and LGWT $_W$ methods rigorously treat the vertex parts to the first order in v (Fig. 2(a)) and in W (Fig. 2(b)), respectively. These vertex parts depend fully on the energy and momentum transfers ω and \mathbf{q} at the center (cross) as well as the frequencies and the coordinates at both ends; see Figs. 2(a) and (b).

Moreover, in the LGWT $_v$ method, it is possible to show that there is no interference between the first-order vertex part of Fig. 2(a) (i.e., the vertex part at the first order in v) and Λ_σ in the $\omega = \mathbf{q} = 0$ limit. In the $\omega = \mathbf{q} = 0$ limit, the former can be expressed as the $-\omega$ derivative of the ω -independent Fock exchange self-energy Σ_σ^x and hence exactly equals to zero, i.e., $\Gamma_{v\sigma}(\mathbf{r}_1, \mathbf{r}_2, \mathbf{q} = 0; \epsilon, \epsilon) = -\partial \Sigma_\sigma^x / \partial \omega = 0$. Therefore, the full vertex part Λ_σ in the $\omega = \mathbf{q} = 0$ limit introduced in the linearized formulation does not interfere to the first-order vertex part of Fig. 2(a). In the LGWT $_W$ method, however, the first-order vertex part of Fig. 2(b) (i.e., the vertex part at the first order in W) may interfere with the full vertex part Λ_σ in the $\omega = \mathbf{q} = 0$ limit at higher orders beyond the present approximation.

PROOF OF THEOREM 2

Ward–Takahashi identity [16-18] is given by

$$\begin{aligned} & \delta^4(x_1 - x)G^{-1}(x, x_2) - G^{-1}(x_1, x)\delta^4(x - x_2) \\ &= i\nabla \cdot \mathbf{\Gamma}(x_1, x_2, x) + i\frac{\partial}{\partial t}\Gamma(x_1, x_2, x). \end{aligned} \quad (\text{S.5})$$

If we Fourier transform this equation with respect to $t - t_2$ and $t_1 - t$ into $\epsilon + \omega$ and ϵ , respectively, (i.e., if we multiply $\exp[i(\epsilon + \omega)(t - t_2) + i\epsilon(t_1 - t)]$ and integrate with respect to $t - t_1$ and $t_1 - t$), this equation becomes

$$\begin{aligned} & \delta(\mathbf{r}_1 - \mathbf{r})G^{-1}(\mathbf{r}_1, \mathbf{r}_2; \epsilon + \omega) - G^{-1}(\mathbf{r}_1, \mathbf{r}_2; \epsilon)\delta(\mathbf{r} - \mathbf{r}_2) \\ &= i\nabla \cdot \mathbf{\Gamma}(\mathbf{r}_1, \mathbf{r}_2, \mathbf{r}; \epsilon + \omega, \epsilon) + \omega\Gamma(\mathbf{r}_1, \mathbf{r}_2, \mathbf{r}; \epsilon + \omega, \epsilon). \end{aligned} \quad (\text{S.6})$$

At the lowest order, the first term in the right hand side is approximately given by

$$\begin{aligned}
& i\nabla \cdot \mathbf{\Gamma}(\mathbf{r}_1, \mathbf{r}_2, \mathbf{r}; \epsilon + \omega, \epsilon) \\
& \sim \frac{1}{2} \nabla \cdot (\nabla_1 + \nabla_2) \delta(\mathbf{r}_1 - \mathbf{r}) \delta(\mathbf{r} - \mathbf{r}_2) \\
& = -\delta(\mathbf{r}_1 - \mathbf{r}) \frac{1}{2} \nabla^2 \delta(\mathbf{r} - \mathbf{r}_2) + \frac{1}{2} \nabla_1^2 \delta(\mathbf{r}_1 - \mathbf{r}) \delta(\mathbf{r} - \mathbf{r}_2) \\
& \quad -i \int_{-\infty}^{\infty} \frac{d\omega'}{2\pi} G(\mathbf{r}_1, \mathbf{r}; \epsilon - \omega') \left(-\frac{1}{2} \nabla^2 \right) G(\mathbf{r}, \mathbf{r}_2; \epsilon + \omega - \omega') W(\mathbf{r}_1, \mathbf{r}_2; \omega') \\
& \quad +i \int_{-\infty}^{\infty} \frac{d\omega'}{2\pi} \left(-\frac{1}{2} \nabla_1^2 \right) G(\mathbf{r}_1, \mathbf{r}; \epsilon - \omega') G(\mathbf{r}, \mathbf{r}_2; \epsilon + \omega - \omega') W(\mathbf{r}_1, \mathbf{r}_2; \omega').
\end{aligned} \tag{S.7}$$

Substituting this into (S.6), we have

$$\begin{aligned}
& \delta(\mathbf{r}_1 - \mathbf{r}) G^{-1}(\mathbf{r}_1, \mathbf{r}_2; \epsilon + \omega) - G^{-1}(\mathbf{r}_1, \mathbf{r}_2; \epsilon) \delta(\mathbf{r} - \mathbf{r}_2) \\
& = -\delta(\mathbf{r}_1 - \mathbf{r}) \frac{1}{2} \nabla^2 \delta(\mathbf{r} - \mathbf{r}_2) + \frac{1}{2} \nabla_1^2 \delta(\mathbf{r}_1 - \mathbf{r}) \delta(\mathbf{r} - \mathbf{r}_2) \\
& \quad -i \int_{-\infty}^{\infty} \frac{d\omega'}{2\pi} G(\mathbf{r}_1, \mathbf{r}; \epsilon - \omega') \left(-\frac{1}{2} \nabla^2 \right) G(\mathbf{r}, \mathbf{r}_2; \epsilon + \omega - \omega') W(\mathbf{r}_1, \mathbf{r}_2; \omega') \\
& \quad +i \int_{-\infty}^{\infty} \frac{d\omega'}{2\pi} \left(-\frac{1}{2} \nabla_1^2 \right) G(\mathbf{r}_1, \mathbf{r}; \epsilon - \omega') G(\mathbf{r}, \mathbf{r}_2; \epsilon + \omega - \omega') W(\mathbf{r}_1, \mathbf{r}_2; \omega') \\
& \quad +\omega \Gamma(\mathbf{r}_1, \mathbf{r}_2, \mathbf{r}; \epsilon + \omega, \epsilon),
\end{aligned} \tag{S.8}$$

which is equivalent to

$$\begin{aligned}
& \Sigma(\mathbf{r}_1, \mathbf{r}_2; \epsilon) \delta(\mathbf{r} - \mathbf{r}_2) - \delta(\mathbf{r}_1 - \mathbf{r}) \Sigma(\mathbf{r}_1, \mathbf{r}_2; \epsilon + \omega) \\
& = -i \int_{-\infty}^{\infty} \frac{d\omega'}{2\pi} G(\mathbf{r}_1, \mathbf{r}; \epsilon - \omega') \left(-\frac{1}{2} \nabla^2 \right) G(\mathbf{r}, \mathbf{r}_2; \epsilon + \omega - \omega') W(\mathbf{r}_1, \mathbf{r}_2; \omega') \\
& \quad +i \int_{-\infty}^{\infty} \frac{d\omega'}{2\pi} \left(-\frac{1}{2} \nabla_1^2 \right) G(\mathbf{r}_1, \mathbf{r}; \epsilon - \omega') G(\mathbf{r}, \mathbf{r}_2; \epsilon + \omega - \omega') W(\mathbf{r}_1, \mathbf{r}_2; \omega') \\
& \quad +\omega [\Gamma(\mathbf{r}_1, \mathbf{r}_2, \mathbf{r}; \epsilon + \omega, \epsilon) - \delta(\mathbf{r}_1 - \mathbf{r}) \delta(\mathbf{r} - \mathbf{r}_2)].
\end{aligned} \tag{S.9}$$

In the linearized formulation, this equation can be rewritten as

$$\begin{aligned}
& \Sigma(\mathbf{r}_1, \mathbf{r}_2; \epsilon) \delta(\mathbf{r} - \mathbf{r}_2) - \delta(\mathbf{r}_1 - \mathbf{r}) \Sigma(\mathbf{r}_1, \mathbf{r}_2; \epsilon + \omega) \\
& = -i \int_{-\infty}^{\infty} \frac{d\omega'}{2\pi} \tilde{G}(\mathbf{r}_1, \mathbf{r}; \epsilon - \omega') \left(-\frac{1}{2} \nabla^2 \right) \tilde{G}(\mathbf{r}, \mathbf{r}_2; \epsilon + \omega - \omega') W(\mathbf{r}_1, \mathbf{r}_2; \omega') \\
& \quad +i \int_{-\infty}^{\infty} \frac{d\omega'}{2\pi} \left(-\frac{1}{2} \nabla_1^2 \right) \tilde{G}(\mathbf{r}_1, \mathbf{r}; \epsilon - \omega') \tilde{G}(\mathbf{r}, \mathbf{r}_2; \epsilon + \omega - \omega') W(\mathbf{r}_1, \mathbf{r}_2; \omega') \\
& \quad +\omega [\Gamma(\mathbf{r}_1, \mathbf{r}_2, \mathbf{r}; \epsilon + \omega, \epsilon) - \delta(\mathbf{r}_1 - \mathbf{r}) \delta(\mathbf{r} - \mathbf{r}_2)].
\end{aligned} \tag{S.10}$$

In order to prove this equality, we calculate the left hand side of (S.10) within the linearized formulation as follows:

$$\begin{aligned}
& i \int_{-\infty}^{\infty} \frac{d\omega'}{2\pi} [\tilde{G}(\mathbf{r}_1, \mathbf{r}_2; \epsilon - \omega') \delta(\mathbf{r} - \mathbf{r}_2) - \delta(\mathbf{r}_1 - \mathbf{r}) \tilde{G}(\mathbf{r}_1, \mathbf{r}_2; \epsilon + \omega - \omega')] W(\mathbf{r}_1, \mathbf{r}_2; \omega') \\
&= i \int_{-\infty}^{\infty} \frac{d\omega'}{2\pi} \left[\langle \mathbf{r}_1 | \frac{1}{\epsilon - \omega' - \tilde{H} - i\delta_{\tilde{H}}} | \mathbf{r} \rangle \langle \mathbf{r} | \mathbf{r}_2 \rangle - \langle \mathbf{r}_1 | \mathbf{r} \rangle \langle \mathbf{r} | \frac{1}{\epsilon + \omega - \omega' - \tilde{H} - i\delta_{\tilde{H}}} | \mathbf{r}_2 \rangle \right] W(\mathbf{r}_1, \mathbf{r}_2; \omega') \\
&= i \int_{-\infty}^{\infty} \frac{d\omega'}{2\pi} \langle \mathbf{r}_1 | \frac{1}{\epsilon - \omega' - \tilde{H} - i\delta_{\tilde{H}}} | \mathbf{r} \rangle \langle \mathbf{r} | \frac{\epsilon + \omega - \omega' - \tilde{H} - i\delta_{\tilde{H}}}{\epsilon + \omega - \omega' - \tilde{H} - i\delta_{\tilde{H}}} | \mathbf{r}_2 \rangle W(\mathbf{r}_1, \mathbf{r}_2; \omega') \\
&\quad - i \int_{-\infty}^{\infty} \frac{d\omega'}{2\pi} \langle \mathbf{r}_1 | \frac{\epsilon - \omega' - \tilde{H} - i\delta_{\tilde{H}}}{\epsilon - \omega' - \tilde{H} - i\delta_{\tilde{H}}} | \mathbf{r} \rangle \langle \mathbf{r} | \frac{1}{\epsilon + \omega - \omega' - \tilde{H} - i\delta_{\tilde{H}}} | \mathbf{r}_2 \rangle W(\mathbf{r}_1, \mathbf{r}_2; \omega') \\
&= i \int_{-\infty}^{\infty} \frac{d\omega'}{2\pi} \langle \mathbf{r}_1 | \frac{1}{\epsilon - \omega' - \tilde{H} - i\delta_{\tilde{H}}} | \mathbf{r} \rangle \langle \mathbf{r} | \frac{\omega}{\epsilon + \omega - \omega' - \tilde{H} - i\delta_{\tilde{H}}} | \mathbf{r}_2 \rangle W(\mathbf{r}_1, \mathbf{r}_2; \omega') \\
&\quad - i \int_{-\infty}^{\infty} \frac{d\omega'}{2\pi} \langle \mathbf{r}_1 | \frac{1}{\epsilon - \omega' - \tilde{H} - i\delta_{\tilde{H}}} | \mathbf{r} \rangle \langle \mathbf{r} | \tilde{H} \frac{1}{\epsilon + \omega - \omega' - \tilde{H} - i\delta_{\tilde{H}}} | \mathbf{r}_2 \rangle W(\mathbf{r}_1, \mathbf{r}_2; \omega') \\
&\quad + i \int_{-\infty}^{\infty} \frac{d\omega'}{2\pi} \langle \mathbf{r}_1 | \tilde{H} \frac{1}{\epsilon - \omega' - \tilde{H} - i\delta_{\tilde{H}}} | \mathbf{r} \rangle \langle \mathbf{r} | \frac{1}{\epsilon + \omega - \omega' - \tilde{H} - i\delta_{\tilde{H}}} | \mathbf{r}_2 \rangle W(\mathbf{r}_1, \mathbf{r}_2; \omega') \\
&= i\omega \int_{-\infty}^{\infty} \frac{d\omega'}{2\pi} \tilde{G}(\mathbf{r}_1, \mathbf{r}; \epsilon - \omega') \tilde{G}(\mathbf{r}, \mathbf{r}_2; \epsilon + \omega - \omega') W(\mathbf{r}_1, \mathbf{r}_2; \omega') \\
&\quad - i \int_{-\infty}^{\infty} \frac{d\omega'}{2\pi} \tilde{G}(\mathbf{r}_1, \mathbf{r}; \epsilon - \omega') \left(-\frac{1}{2} \nabla^2 \right) \tilde{G}(\mathbf{r}, \mathbf{r}_2; \epsilon + \omega - \omega') W(\mathbf{r}_1, \mathbf{r}_2; \omega') \\
&\quad + i \int_{-\infty}^{\infty} \frac{d\omega'}{2\pi} \left(-\frac{1}{2} \nabla_1^2 \right) \tilde{G}(\mathbf{r}_1, \mathbf{r}; \epsilon - \omega') \tilde{G}(\mathbf{r}, \mathbf{r}_2; \epsilon + \omega - \omega') W(\mathbf{r}_1, \mathbf{r}_2; \omega') \\
&\quad - i \int_{-\infty}^{\infty} \frac{d\omega'}{2\pi} \int d\mathbf{r}' \tilde{G}(\mathbf{r}_1, \mathbf{r}; \epsilon - \omega') \Sigma_{xc}(\mathbf{r}, \mathbf{r}') \tilde{G}(\mathbf{r}', \mathbf{r}_2; \epsilon + \omega - \omega') W(\mathbf{r}_1, \mathbf{r}_2; \omega') \\
&\quad + i \int_{-\infty}^{\infty} \frac{d\omega'}{2\pi} \int d\mathbf{r}' \Sigma_{xc}(\mathbf{r}_1, \mathbf{r}') \tilde{G}(\mathbf{r}', \mathbf{r}; \epsilon - \omega') \tilde{G}(\mathbf{r}, \mathbf{r}_2; \epsilon + \omega - \omega') W(\mathbf{r}_1, \mathbf{r}_2; \omega'), \tag{S.11}
\end{aligned}$$

where we used the fact that the electron-nucleus potential in \tilde{H} commutes with the operator $|\mathbf{r}\rangle\langle\mathbf{r}|$. The first term of Eq. (S.11) is exactly equal to the vertex part at the lowest order in the dynamically screened Coulomb interaction W shown in Fig. 2(b) except for the prefactor ω , and thus equals to the last two terms of the right hand side of Eq. (S.10). The second and the third terms equal to the first and second terms of the right hand side of Eq. (S.10). The fourth and fifth terms are at least one order higher in v compared to the other terms that are lowest order in W , and can be ignored. Therefore, the LGWT_W method satisfies the Ward–Takahashi identity to the lowest order in W . This discussion holds also in the case we expand to the first order in the electron-electron Coulomb interaction v of Fig. 2(a), since $W(\mathbf{r}_1, \mathbf{r}_2; \omega')$ can be replaced by $v(\mathbf{r}_1 - \mathbf{r}_2)$ in this case. Therefore, the LGWT_v method also satisfies the Ward–Takahashi identity to the lowest order in v .

POLARIZATION FUNCTION AND SELF-ENERGY

The contributions to the polarization function and self-energy coming from the first-order vertex correction, FIGs. 2(e) and (h) are explicitly given by

$$\begin{aligned} \widetilde{P}_{GG'}^{(1)}(\omega) = & \frac{1}{\Omega} \int \frac{d\omega'}{2\pi} e^{i\omega'\eta} \int \frac{d\omega''}{2\pi} e^{i\omega''\eta} \sum_{\sigma} \sum_{ijkl} \sum_{G''G'''} W_{G''G'''}(\omega'') \\ & \times \frac{\langle \widetilde{i\sigma} | e^{-i\mathbf{G}\cdot\mathbf{r}} | \widetilde{j\sigma} \rangle \langle \widetilde{j\sigma} | e^{-i\mathbf{G}''\cdot\mathbf{r}''} | \widetilde{k\sigma} \rangle \langle \widetilde{k\sigma} | e^{i\mathbf{G}'\cdot\mathbf{r}'} | \widetilde{l\sigma} \rangle \langle \widetilde{l\sigma} | e^{i\mathbf{G}'''\cdot\mathbf{r}'''} | \widetilde{i\sigma} \rangle}{(\omega' - \epsilon_{i\sigma} - i\eta_{i\sigma})(\omega + \omega' - \epsilon_{j\sigma} - i\eta_{j\sigma})(\omega' + \omega'' + \omega - \epsilon_{k\sigma} - i\eta_{k\sigma})(\omega' + \omega'' - \epsilon_{l\sigma} - i\eta_{l\sigma})}, \end{aligned} \quad (\text{S.12})$$

and

$$\begin{aligned} (\alpha | \Sigma_{\sigma}^{(2)}(\omega) | \beta) = & \int \frac{d\omega'}{2\pi} e^{i\omega'\eta} \int \frac{d\omega''}{2\pi} e^{i\omega''\eta} \sum_{\sigma} \sum_{ijk} \sum_{GG'} \sum_{G''G'''} W_{GG'}(\omega') W_{G''G'''}(\omega'') \\ & \times \frac{(\alpha | e^{i\mathbf{G}\cdot\mathbf{r}} | \widetilde{i\sigma}) \langle \widetilde{i\sigma} | e^{i\mathbf{G}'\cdot\mathbf{r}'} | \widetilde{j\sigma} \rangle \langle \widetilde{j\sigma} | e^{-i\mathbf{G}''\cdot\mathbf{r}''} | \widetilde{k\sigma} \rangle \langle \widetilde{k\sigma} | e^{-i\mathbf{G}'''\cdot\mathbf{r}'''} | \beta \rangle}{(\omega + \omega' - \epsilon_{i\sigma} - i\eta_{i\sigma})(\omega + \omega' + \omega'' - \epsilon_{j\sigma} - i\eta_{j\sigma})(\omega + \omega'' - \epsilon_{k\sigma} - i\eta_{k\sigma})}, \end{aligned} \quad (\text{S.13})$$

respectively, where $W_{GG'}(\omega)$ is the dynamically screened Coulomb interaction, η is a positive infinitesimal ($\eta_{i\sigma}$ is η for occupied $i\sigma$ and $-\eta$ for empty $i\sigma$), Ω is the volume of the unit cell, and $(\alpha |, | \beta)$ denote basis functions.

INTERACTION KERNEL $\widetilde{I}_{\nu\mu dc}^{\sigma_1\sigma'_1}(\omega)$

As written in the Letter, the interaction kernel $\widetilde{I}^{\sigma_3\sigma'_3}(x_3, x'_3; x_4, x'_4)$ is expressed as $i\{\delta(x_3 - x_4)\delta(x'_3 - x'_4)W(x_3, x'_3) + \delta(x_3 - x_4)[W\Gamma_{\nu\sigma_3}](x'_3, x'_4; x_3) + \delta(x'_3 - x'_4)[W\Gamma_{\nu\sigma_3}](x_3, x_4; x'_3)\}$, which are diagrammatically represented by Figs. 2(i), (j), and (k), respectively. In the third term corresponding to Fig. 2(k), for example, the two points connected by the dotted line, i.e., the bare Coulomb interaction, are the same time $t_3 = t_4$. On the other hand, one end of the wavy line, which is involved in this vertex part $\Gamma_{\nu\sigma_3}$ is another time, say t'' , and the other end of the wavy line, which is not involved in the vertex part is obviously a unique time $t'_3 = t'_4$. Therefore, this interaction kernel $\widetilde{I}^{\sigma_3\sigma'_3}(x_3, x'_3; x_4, x'_4)$ has only the time dependence through $\tau = t_3 - t'_3$. Moreover, the vertex part $\Gamma_{\nu\sigma_3}$ in this diagram has only the time dependence through $\tau' = t_3 - t''$, and the wavy line W has only the time dependence through $\tau'' = t'' - t'_3 = \tau - \tau'$. Therefore, the interaction kernel $\widetilde{I}^{\sigma_3\sigma'_3}(\tau)$, i.e., the dynamically screened Coulomb interaction $W(\tau - \tau')$ times the vertex correction $\Gamma_{\nu\sigma_3}(\tau')$, has

a convolution type in time, so that its Fourier transformation from τ to ω' is written as $\widetilde{I}^{\sigma_3\sigma'_3}(\omega')$, which can be written as the product of the Fourier transforms of $W(\tau')$ and $\Gamma_{v\sigma_3}(\tau')$, $W(\omega')$ and $\Gamma_{v\sigma_3}(\omega')$; thus we have $\widetilde{I}^{\sigma_3\sigma'_3}(\omega') = W(\omega')\Gamma_{v\sigma_3}(\omega')$. Since the ω' -dependence in $\widetilde{I}^{\sigma_3\sigma'_3}(\omega')$ can be treated in a standard way given first by Strinati [S1] when we solve the Bethe–Salpeter equation, it is allowed to replace $\widetilde{I}^{\sigma_3\sigma'_3}(\omega')$ with $W(\omega')\Gamma_{v\sigma_3}(\omega')$ in the final equation (2.18) of Ref. [S1], and thus we can derive

$$\begin{aligned} \widetilde{I}_{v\mu dc}^{\sigma_1\sigma'_1}(\omega) = & i \sum_{GG'} \int \frac{d\omega'}{2\pi} e^{-i\omega'\eta} W_{GG'}(\omega') \left\{ \langle \widetilde{v\sigma_1} | e^{iG \cdot r} | c\sigma_1 \rangle \langle d\sigma'_1 | e^{-iG' \cdot r'} | \widetilde{\mu\sigma'_1} \rangle \right. \\ & + \sum_{\alpha\beta} (\delta_{\alpha \text{ occ}} \delta_{\beta \text{ emp}} - \delta_{\alpha \text{ emp}} \delta_{\beta \text{ occ}}) \left(\langle \widetilde{v\sigma_1} | e^{iG \cdot r} | c\sigma_1 \rangle V_{d\alpha\beta\mu}^{\sigma'_1\sigma'_1} \frac{\langle \widetilde{\alpha\sigma'_1} | e^{-iG' \cdot r'} | \widetilde{\beta\sigma'_1} \rangle}{\epsilon_{\alpha\sigma'_1} - \epsilon_{\beta\sigma'_1} + \omega' + i\eta_{\alpha\sigma'_1}} \right. \\ & \left. \left. + V_{v\alpha\beta c}^{\sigma_1\sigma_1} \frac{\langle \widetilde{\alpha\sigma_1} | e^{iG \cdot r} | \widetilde{\beta\sigma_1} \rangle}{\epsilon_{\alpha\sigma_1} - \epsilon_{\beta\sigma_1} - \omega' + i\eta_{\alpha\sigma_1}} \langle d\sigma'_1 | e^{-iG' \cdot r'} | \widetilde{\mu\sigma'_1} \rangle \right) \right\} \\ & \times \left\{ \frac{1}{\omega - \omega' - \epsilon_{c\sigma_1} + \epsilon_{\mu\sigma'_1} + i\eta} + \frac{1}{\omega + \omega' - \epsilon_{v\sigma_1} + \epsilon_{d\sigma'_1} + i\eta} \right\} \end{aligned} \quad (\text{S.14})$$

with $V_{v\mu dc}^{\sigma_1\sigma_2} = \sum_G \langle \widetilde{v\sigma_1} | e^{iG \cdot r} | \widetilde{\mu\sigma_1} \rangle \langle d\sigma_2 | e^{-iG \cdot r'} | c\sigma_2 \rangle v(G)$ (note that all states are renormalized QP states except for d and c).

Reference:

[S1] G. Strinati, Phys. Rev. B **29**, 5718 (1984).